Development and Application of Position-Sensitive Double Parallel-Plate Avalanche Counter*

Chen Yuan,[1,2] Fu-Shuai Shi,[1,2,†] Xiao-Dong Xu,[1,2] Zhi-Chao Zhang,[1] En-Qiang Liu,[1] He-Run Yang,[3,2,‡] Peng Ma,[4,3,2,§] Li-Min Duan,[3,2] Hooi-Jin Ong,[1,2,5,6,7,¶] Satoru Terashima,[1,2,6,7] Ze-Yu Du,[8] Zhi-Heng Hu,[1,2] Tai-Sen Huang,[1,2] Lu Li,[1,2] Peng-Jie Li,[9] Hong-Na Liu,[10] Bing-Feng Lv,[1,2] Jun-Bing Ma,[1] Zi-Xu Ma,[1,2] Ye-Lei Sun,[11] He Wang,[1,2] Xiang-Lun Wei,[3,2] Zai-Hong Yang,[8] and Wei-Dong Zhang[1,2]

[1]*State Key Laboratory of Heavy Ion Science and Technology, Institute of Modern Physics, Chinese Academy of Sciences, Lanzhou 730000, China*
[2]*School of Nuclear Science and Technology, University of Chinese Academy of Sciences, Beijing 100049, China*
[3]*Institute of Modern Physics, Chinese Academy of Sciences, Lanzhou 730000, China*
[4]*Present address: Shandong Provincial Key Laboratory of Nuclear Science, Nuclear Energy Technology and Comprehensive Utilization, School of Nuclear Science, Energy and Power Engineering, Shandong University, Jinan 250061, China*
[5]*Joint Department for Nuclear Physics, Lanzhou University and Institute of Modern Physics, Chinese Academy of Sciences, Lanzhou 730000, China*
[6]*Research Center for Nuclear Physics, Osaka University, Ibaraki, Osaka 567-0047, Japan*
[7]*Nishina Center for Accelerator-Based Science, RIKEN, 2-1 Hirosawa, Wako, 351-0198 Saitama, Japan*
[8]*School of Physics and State Key Laboratory of Nuclear Physics and Technology, Peking University, Beijing 100871, China*
[9]*Key Laboratory of Nuclear Physics and Ion-beam Application (MOE), Institute of Modern Physics, Fudan University, Shanghai 200433, China*
[10]*School of Physics and Astronomy, Beijing Normal University, Beijing 100875, China*
[11]*School of Physics, Beihang University, Beijing 100191, China*

Double parallel-plate avalanche counters (DPPACs), each comprising two PPACs with delay-line readout for two-dimensional position determination, have been developed at Institute of Modern Physics, Chinese Academy of Sciences. The detector was tested with a standard α source, achieving a position resolution of about 0.4 mm. Each PPAC measures particle hit positions in two dimensions, with the dual configuration enhancing overall detection efficiency. Two DPPACs were deployed in a month-long experimental campaign at the Radioactive Ion Beam Line in Lanzhou (RIBLL1) with secondary beams of ^{10}C, ^{10}Be, ^{11}C and ^{16}C at typical intensities of 1.2 – 1.5 $\times 10^5$ Hz, yielding a stable single DPPAC-detection efficiency >90% and a typical in-beam position resolution $\approx$ 0.54 mm.

Keywords: Radioactive isotope beam; Parallel-plate avalanche counter; Delay-line readout; Position resolution; Detection efficiency

I. INTRODUCTION

Advances in radioactive ion beam (RIB) technology have driven the construction of major international facilities, including RI Beam Factory (RIBF) in Japan [1], the Facility for Antiproton and Ion Research (FAIR) in Europe [2], and the Facility for Rare Isotope Beams (FRIB) in the US [3]. In China, Radioactive Ion Beam Lines in Lanzhou (RIBLL1 and RIBLL2) [4–7] at Heavy Ion Research Facility in Lanzhou (HIRFL) have served as the core domestic platforms for performing RIB physics experiments. This role will be (partially) assumed by the next-generation HIgh Rigidity Ion Beam Line (HIRIBL), formerly HFRS [8, 9], at the recently commissioned High-Intensity heavy-ion Accelerator Facility (HIAF) in Huizhou [10]. These facilities enable synthesis of exotic nuclides near drip lines, unlocking vast potentials to advance key frontiers in nuclear physics and nuclear astrophysics, including r-process pathways [11, 12], exotic nuclear structures from weak binding (e.g., neutron/proton halos, neutron skins [13, 14]), and shell evolution under extreme isospin asymmetry [15–17].

A typical RIB experiment involves the production, selection, and separation of secondary beams, followed by their transport to the experimental area where they impinge on a reaction target or an active stopper. Such experiments, however, face several inherent challenges. RIBs generally exhibit large emittance and energy spread, together with relatively low beam intensities, which severely limits the achievable statistics and hampers high-precision nuclear spectroscopy studies based on nuclear reactions. In addition to precise kinetic-energy measurements, an accurate determination of differential cross sections demands high-resolution, event-by-event tracking of both incident beam particles and reaction products, in order to reconstruct their hit positions on the tar-

* Supported by the National Natural Science Foundation of China (Nos. 12175280, 12175009, 12250610193 and 12505146), the Project of Top-notch Leading Talents in Gansu Province, the Research Program of Heavy Ion Science and Technology Key Laboratory, Institute of Modern Physics, Chinese Academy of Sciences (HIST2025KS01), the CAS "Global Initiative on Common Challenges" under Contract No. 016GJHZ2023063GC, Major Science and Technology Projects in Gansu Province under Grant No. 24GD13GA005, and the CAS "Light of West China" Program.

† Fu-Shuai Shi and Chen Yuan contributed equally to this work, and should be considered as co-first authors.
‡ Corresponding author: Yang Herun, Nanchang Road 509, Lanzhou 730000, yanghr@impcas.ac.cn
§ Corresponding author: Ma Peng, Nanchang Road 509, Lanzhou 730000, mapeng@sdu.edu.cn
¶ Corresponding author: Ong Hooi Jin, Nanchang Road 509, Lanzhou 730000, onghjin@impcas.ac.cn

get or stopper and to determine their incident and scattering angles with high precision.

Conventional position-sensitive gaseous detectors, such as multi-wire drift chambers [18–20] (MWDCs), parallel plate avalanche counters [21–25] (PPACs) and time-projection chambers [26, 27] (TPCs) have been widely employed for beam diagnostics, secondary-beam identification and particle tracking. MWDCs provide excellent position resolution on the order of 100 μm, but at the expense of complex, multi-channel readout electronics, typically involving several hundred channels per detector. TPCs offer good three-dimensional position resolution, but require sophisticated mechanical designs, intricate readout systems, and are vulnerable to space-charge effects at high rate; further developments are underway to enhance their rate capability [28, 29]. Alternative options include position-sensitive ionization chambers [30, 31] (PSICs), fiber scintillators [32, 33] and silicon microstrip detectors [34]. PSICs enable reliable Z identification but only moderate position resolution ($\sim$ 1 mm); fiber scintillators deliver fast timing and modest position resolution, though large-area implementations with fine granularity necessitate extensive channels and precise optical coupling; silicon microstrip detectors achieve exceptional energy and position resolution (a few hundred μm), but suffer from radiation damage and high costs for broad coverage. In this context, delay-line readout PPACs offer a particularly attractive compromise, combining fast timing (a few hundred ps), sub-mm position resolution, and high efficiency for heavy-ion detection with simple, cost-effective construction, making them a versatile and widely favored instrument for intermediate- and low-energy heavy-ion measurements.

The parallel-plate avalanche counter (PPAC), first proposed by J. Christiansen in 1952 [35], has become a standard position-sensitive detector for beam diagnostics at major international RIB facilities [23–25]. In China, PPACs of the double-grid type [36] – featuring a cathode plane of double-sided aluminized Mylar foil glued between two epoxy frames, sandwiched between two gold-plated tungsten-wire anode planes – were developed [37, 38] at the Institute of Modern Physics, Chinese Academy of Sciences. These detectors have been deployed in heavy-ion collission experiments at RIBLL1 to track fission products [39–41], as well as for beam diagnostics in RIB experiments [42–46]. While fulfilling the requirements for fission-product tracking, the detectors exhibited vulnerability to discharge under increasing radiation doses, leading to deteriorating detection efficiencies [47].

In this article, we report on the construction and application of double parallel-plate avalanche counters (DPPACs) with delay-line readout for RIB experiments. A prototype PPAC was recently constructed and tested with a standard α source [48]. Here, we describe a dual-unit DPPAC system, which houses two PPACs similar to the design in Ref. [23], developed to boost detection efficiency and provide high-precision position measurements of RIBs at the RIBLL facility, with potential deployment at HIAF–HIRIBL. Section II details the detector structure and operating principle, including the gas-flow system, delay-line circuit, conventional readout electronics, and the concept of double PPACs. Section III presents laboratory tests of position resolution using a standard α source. Two DPPACs were deployed during a month-long campaign at RIBLL1 with secondary ^{10}Be and ^{10,11,16}C beams; their in-beam detection efficiency and typical position resolution are presented in Sec. IV. A summary follows in Sec.V.

II. STRUCTURE AND OPERATION PRINCIPLES

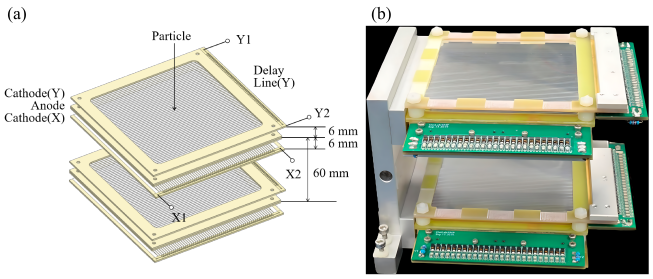

Fig. 1. (a) Schematic of the DPPAC electrode structure. (b) Photograph of the assembled DPPAC. The distance between two PPACs is 60 mm. The active area is 63 mm $\times$ 63 mm.

The electrode structure of the DPPAC is shown in Fig. 1. Each PPAC comprises three parallel frames: a central anode flanked by X- and Y-axis cathode electrodes, ensuring a uniform electric field. The electrodes are fabricated by vacuum evaporation of aluminum onto thin polyester (Mylar) films, which are stretched and glued to 2-mm-thick G10 frame plates using non-conductive adhesive. The anode consists of a 2-μm-thick double-sided aluminized Mylar film sandwiched between two G10 frames. The cathodes feature 1.2-mm-wide aluminum strips (1.27-mm pitch and 70-μm inter-strip gaps) deposited on one side of the film. Compared to double-grid PPACs, this stripline design yields a more uniform electric field. Each cathode film has 50 strips, defining a 63 mm $\times$ 63 mm sensitive area. The inter-electrode spacing is 6 mm. Two PPACs are mounted 60 mm apart inside an aluminum housing with entrance and exit windows on opposing sides. Both windows use 2-μm-thick double-sided aluminized Mylar films, capable of withstanding 50 mbar overpressure.

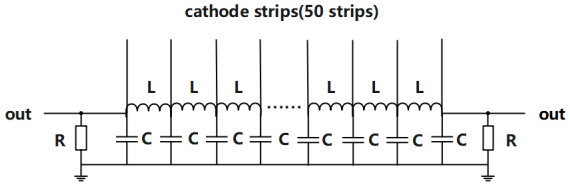

Fig. 2. The equivalent circuit for the delay-line LC circuit board of the PPAC detector. The capacitance, inductance, and resistance are $C = 39$ pF, $L = 95$ nH and $R = 51$ kΩ, respectively.

In delay-line PPACs, position information is determined from cathode timing signals. The delay lines were constructed using a series of commercial chip inductors ($L = 95$ nH, 10% tolerance) and chip capacitors ($C = 39$ pF, 5% tolerance) from Murata Manufacturing Co., Ltd. An equivalent LC circuit is given in Fig. 2. The LC delay-line circuit board is connected to the cathode strips, with an average delay per cell of about 2 ns. Two terminal resistors, with $R = 51$ kΩ, mitigate surface charge buildup, and each cathode strip couples capacitively to a metal sheet on the LC board for readout at both ends. Avalanche-induced cathode signals split bidirectionally along the delay line, reaching the X_1/X_2 (Y_1/Y_2) terminals (see Fig. 1). A time-to-digital converter (TDC), triggered by the anode signal and stopped by both cathode-end signals, yields arrival times used to compute coordinates:

$$\begin{aligned} X &= K_X(T_{X_2} - T_{X_1}) + X_{\text{off}}, \\ Y &= K_Y(T_{Y_2} - T_{Y_1}) + Y_{\text{off}}, \end{aligned} \tag{1}$$

where $K_{X,Y}$ (mm/ns) are calibration coefficients, $T_{X_{1,2}}$ and $T_{Y_{1,2}}$ are end-arrival times, and X_{off} and Y_{off} (mm) are delay-line offsets.

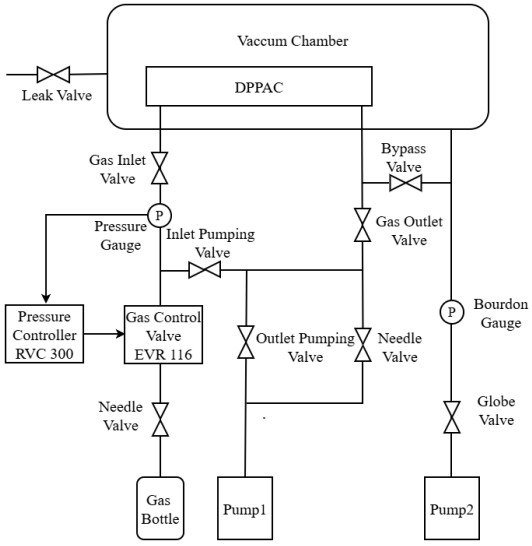

Fig. 3. Schematic of the DPPAC gas-flow system.

The detector is filled with pure isobutane, chosen for its good stability, high gain, favorable signal-to-noise ratio, and relatively low operating voltage, which are particularly advantageous for heavy-ion detection. The DPPAC operates at a gas pressure of 10 mbar, with the anode biased at +840 V during measurement with standard α source to obtain sufficiently large signals on both cathodes while avoiding discharges. To suppress impurities originating mainly from outgassing, and to maintain stable avalanche gain and signal amplitude, a dedicated gas-flow system was constructed and implemented. A typical configuration is illustrated in Fig. 3. The working-gas pressure inside the DPPAC is actively regulated and kept stable within 9% using a pressure controller (Pfeiffer RVC 300), a gas control valve (Pfeiffer EVR 116), and two needle valves.

The anode signal is extracted via a high-voltage filter from the HV line and recorded for timing (T_{A}). All anode and cathode (T_{X_1}, T_{X_2}, T_{Y_1}, T_{Y_2}) timing signals are obtained via the following processing chain: pre-amplification using KB7120 (Kaizuworks Co., Ltd.) voltage-sensitive modules mounted directly on the DPPAC housing to maximize signal-to-noise ratio (see Fig. 4(a)), followed by fast-timing amplifiers (ORTEC FTA 810), constant-fraction discriminators (CFDs), NIM-to-ECL logic-signal conversion modules, and finally digitization in a time-to-digital converter (TDC). In addition to serving as the reference timing signal, T_{A} is also used to trigger the data acquisition (DAQ) system. For standard detector tests, the DAQ is handled by a versa module Europa (VME)-based system.

The double-PPAC configuration enables double position detection, enhancing both position resolution and overall detection efficiency. The X (Y)-position and two-dimensional ($X \cap Y$) detection efficiencies of a single PPAC are defined as

$$\eta_{X(Y)} = \frac{N_{X(Y)}}{N_{\text{ref}}}, \quad \eta_{X\cap Y} = \frac{N_{X\cap Y}}{N_{\text{ref}}}, \tag{2}$$

where $N_{X(Y)}$ is the number of valid X (Y)-position events, $N_{X\cap Y}$ is the number of valid two-dimensional events, and N_{ref} is the number of reference events, determined either by a downstream detector or the PPAC anode (T_{A} trigger). Since a position can be provided by either PPAC (assuming independent operation), the DPPAC detection efficiencies are

$$\eta^{\text{DPPAC}}_{X(Y)} = \eta^1_{X(Y)} + \eta^2_{X(Y)} - \eta^1_{X(Y)}\eta^2_{X(Y)}, \tag{3}$$

$$\eta^{\text{DPPAC}}_{X\cap Y} = \eta^1_{X\cap Y} + \eta^2_{X\cap Y} - \eta^1_{X\cap Y}\eta^2_{X\cap Y}, \tag{4}$$

where superscripts “1" and “2" denote the first and second PPACs, respectively. Eqs. 3 and 4 show that a DPPAC detection efficiency of 0.9 can be achieved even if each individual PPAC has only 0.7 efficiency.

III. OFF-BEAM α SOURCE TEST: POSITION CALIBRATION AND RESOLUTION

Measurements were performed with a ^{241}Am α source to calibrate the DPPAC and determine their intrinsic position resolutions. The α source was placed approximately 25 cm from the detector. A printed circuit board with a 6×17 array of 1-mm-diameter holes was mounted at the DPPAC entrance window to collimate the incident α particles, as shown in Fig. 4(a). The hole pattern was designed to accommodate three sets of 34-pin MIL connectors. Calibration of the K_X and K_Y coefficients was carried out using this hole mask, and an additional measurement without the mask was performed to determine the delay-line offsets. The resulting position distribution is shown in Fig. 4(b), where the hole patterns are clearly resolved, demonstrating good position resolution.

We selected the region containing the hole pattern and projected the hits into the X and Y directions, as shown in Fig. 5.

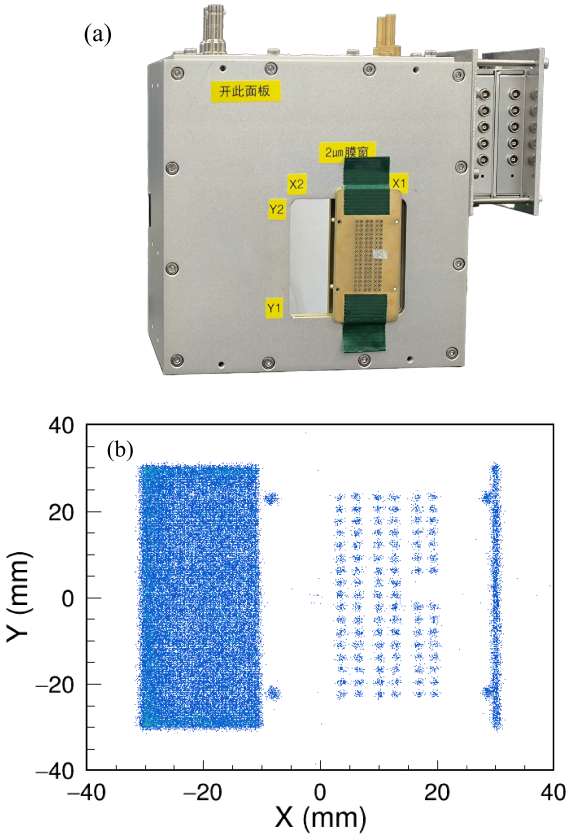

Fig. 4. (a) DPPAC and mask setup for position calibration and resolution measurement. Two pre-amplifiers are mounted on the top right of the DPPAC. (b) Hit pattern measured by the front PPAC in the masked DPPAC detector.

The width and statistical error of each peak were extracted from Gaussian fits. The weighted mean widths for the X and Y directions were calculated to be $\sigma_{\mathrm{meas}X}$ = 0.46 ± 0.01 mm and $\sigma_{\mathrm{meas}Y}$ = 0.48 ± 0.02 mm, where the uncertainties correspond to the weighted standard deviations of the fit errors. Since the α particles passed uniformly through the 1-mm mask holes, with geometric broadening of σ_{geom} = 0.25 mm as estimated by a Monte Carlo simulation, we corrected for this hole contribution using

$$\sigma^2_{\mathrm{meas}} = \sigma^2_{\mathrm{PPAC}} + \sigma^2_{\mathrm{geom}}. \quad (5)$$

The intrinsic position resolutions thus obtained are 0.38 ± 0.01 mm (X) and 0.41 ± 0.03 mm (Y), in root-mean-square (RMS). Unless otherwise noted, all resolutions hereafter are RMS.

IV. PERFORMANCE EVALUATION WITH HIGH-INTENSITY RI BEAMS

The DPPAC detectors were used in a month-long experimental campaign at RIBLL1 with the recently developed liquid-nitrogen-cooled gas target system [49]. Five experiments were performed using secondary ^{10}Be and ^{10,11,16}C beams, produced via projectile-fragmentation reaction of 80-MeV/nucleon ^{12}C and 60-MeV/nucleon ^{18}O primary beams on ^{9}Be targets of 1 – 6-mm thicknesses. Two DPPACs were placed upstream of the gas target to precisely track incident beam trajectories, angles, and hit positions on target; labeled T2-DPPAC and TC-DPPAC, they were spaced 130.0 cm apart, with the former inside RIBLL1's T2 focal-plane vacuum chamber [5], and the latter 31.3 cm upstream of the gas target in the downstream target chamber. Two plastic scintillators were placed in the T1 and T2 chambers to measure the time-of-flight (TOF) of the secondary beams. Two double-sided silicon strip detectors (DSSDs), labeled TG-DSSD and TZ-DSSD, respectively, positioned 2.6 and 30.8 cm downstream of the gas target, detected scattered heavy ions. Instead of the VME system, we employed 16-channel Pixie-16 digital pulse processors (XIA LLC) [50] for the signal digitization and data acquisition to minimize DAQ dead time, with further details in Ref. [51].

Particle identification was performed using the TOF measured by the T1 and T2 plastic scintillators, combined with the energy-loss (ΔE) information from the TZ-DSSD. The default T2 beam-line silicon detector, used for PID during

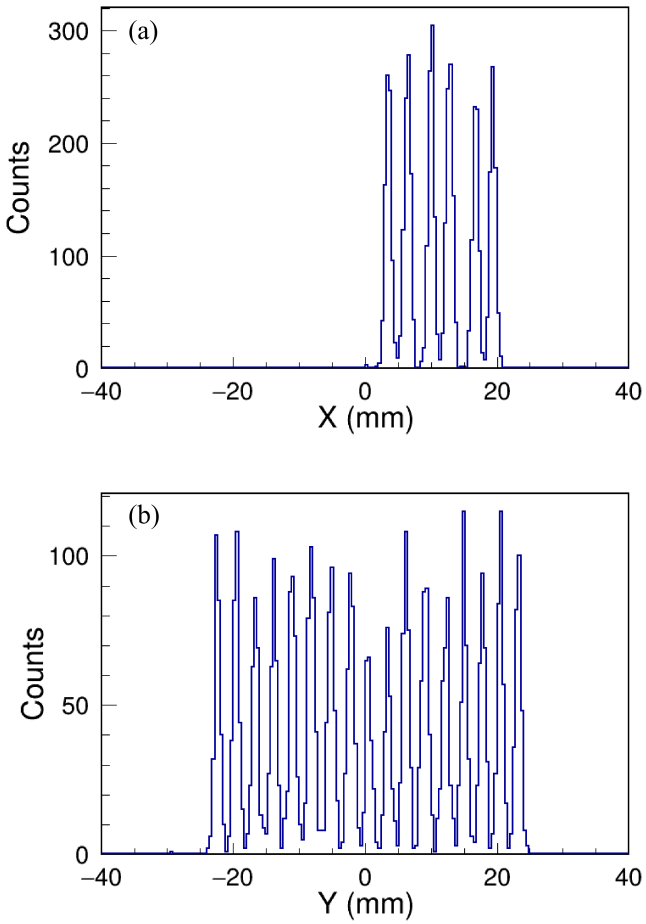

Fig. 5. Collimated α-particle hit positions in the (a) X and (b) Y directions, measured with the mask.

beam tuning, was removed during physics runs. Thus, particle identifications were performed for all beam species using T1–T2 TOF and TZ-DSSD ΔE information. All beam species are well separated.

In the following subsections, we briefly describe the bias voltage optimization, and position resolution determination using the secondary ^{16}C beam as an example. We also present the variation in detection efficiency over the course of the month-long experiments.

A. In-beam detection efficiency and bias voltage optimization

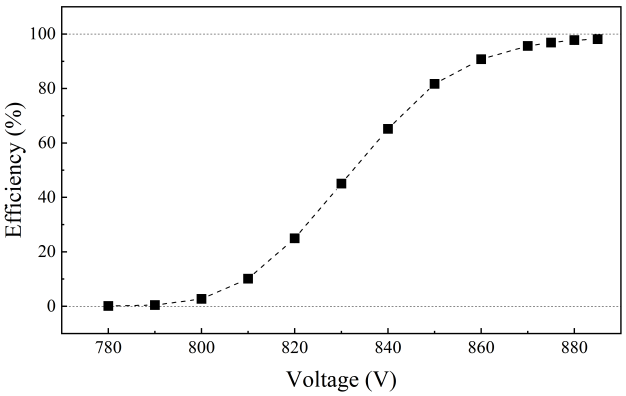

Fig. 6. PPAC4 detection efficiency as a function of voltage for 57-MeV/u ^{16}C ions with 10-mbar isobutane gas. The definition of PPAC4 is given in Sec. IV C.

For each beam setting, we measured the bias-voltage dependent detection efficiency of DPPAC for the selected beam particles to optimize the operating voltage. The number of ^{16}C nuclei identified using the T1-T2 TOF and the TZ-DSSD ΔE was taken as $N_{\rm ref}$ in calculating the detection efficiency. Figure 6 shows a typical efficiency curve of PPAC for 57-MeV/u ^{16}C ions with 10-mbar isobutane as a function of the applied high voltage. We selected an operating voltage range from 780 V to 885 V, recording trigger counts to calculate efficiency in steps of 10 V, with the step size reduced to 5 V when approaching the detector efficiency plateau region. Based on the results of the efficiency curve, 880 V was selected as the operating voltage for the PPAC. The lowest and highest operating voltages among the different beam settings were 820 V (for ^{18}O) and 905 V (for ^{10}Be), respectively.

B. In-beam position resolution

To estimate the in-beam position resolutions, we first reconstructed the incident-beam tracks using hit positions from at least one PPAC in each DPPAC. As noted in Ref. [52], run-dependent timing offsets can occasionally appear in individual channels of the XIA Pixie-16 modules, leading to incorrect position reconstruction. In the present ^{16}C data set, offsets of about 10 ns were observed and corrected using the dedicated reference signals described in Ref. [52]. Gating on ^{16}C particles, we selected single-hit events via $T_{\rm A} - (T_{X(Y)_1} + T_{X(Y)_2})$ and incident angles < 5 mrad, then computed residuals between reconstructed track positions and measured positions. Two classes of residuals were examined: inclusive, for which the measurement from a particular PPAC was used in the track reconstruction, and exclusive, for which it was omitted. The typical widths of the inclusive and exclusive residual distributions were found to be $\sigma_{\rm res;in} \approx 0.45$ mm and $\sigma_{\rm res;ex} \approx 0.70$ mm, respectively. Given that $\sigma_{\rm res;in}$ contains contributions from both the tracking uncertainty ($\sigma_{\rm track}$) and the intrinsic PPAC resolution ($\sigma_{X(Y)}$), whereas $\sigma_{\rm res;ex}$ is independent of $\sigma_{X(Y)}$, it follows that $\sigma_{X(Y)} \approx 0.54$ mm. The estimated in-beam resolution is worse than the intrinsic position resolutions obtained from the α-source test described in Sec. III, likely due to effects such as multiple scattering of beam particles in the detector material between DPPACs, energy loss, multi-hit events, and broadening of the incident angles.

C. One-month operational test: Stability of detection efficiency

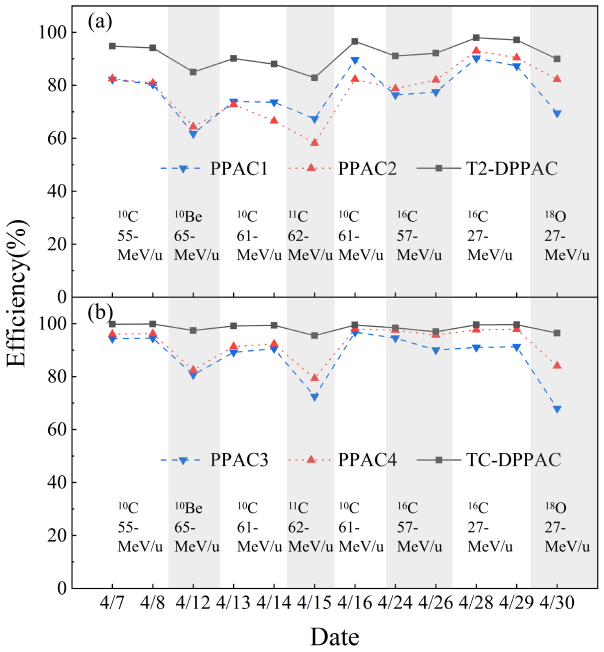

Fig. 7. Variation of PPAC and DPPAC efficiencies over time. The typical rate of the secondary beams was about 1.2 – 1.5 $\times 10^5$ Hz. The bias voltages for PPAC1–PPAC4 were kept slightly below their optimized values during ^{10}Be, ^{11}C and ^{18}O runs to avoid continuous discharge, resulting in lower detection efficiencies.

The detection efficiencies for various beam particles over the course of the experimental campaign were evaluated to assess the stability of the DPPACs. We again took the number of identified beam particles, selected using the T1-T2 TOF and the TZ-DSSD ΔE as $N_{\rm ref}$. For each beam species, we selected one or two data sets from stable physics run containing a sufficiently large number of events. Defining the two PPACs in T2-DPPAC (TC-DPPAC) as PPAC1 and PPAC2 (PPAC3 and PPAC4), we determined $\eta_{X\cap Y}^{\mathrm{PPAC}i}$ $(i = 1, 2, 3, 4)$ as functions of date, as shown in Fig. 7(a) and (b). The white and gray bands indicate different beam settings, with the corresponding beam species and energies labeled. Beam intensities at the RIBLL1-T2 focal plane were typically on the order of 10^5 Hz during physics runs, reaching $\geq 1.6 \times 10^5$ Hz for ^{10}Be and $\geq 2.0 \times 10^5$ Hz for ^{11}C. To avoid continuous discharge, bias voltages were kept slightly below the optimized values during ^{10}Be and ^{11}C runs, and for the faint, focused ^{18}O primary beam, yielding slightly lower detection efficiencies.

Events with valid X and Y positions in either PPAC1 or PPAC2 were used to determine the T2-DPPAC efficiency ($\eta_{X\cap Y}^{\mathrm{T2\text{-}DPPAC}}$), while those with valid positions in PPAC3 or PPAC4 were used for the TC-DPPAC efficiency ($\eta_{X\cap Y}^{\mathrm{TC\text{-}DPPAC}}$). $\eta_{X\cap Y}^{\mathrm{T2\text{-}DPPAC}}$ remained above 90% during most physics runs, dipping slightly to 85% for ^{10}Be and 83% for ^{11}C, respectively. In contrast, $\eta_{X\cap Y}^{\mathrm{TC\text{-}DPPAC}}$ stayed close to 100% throughout the experiments, demonstrating the significant advantage of the DPPAC configuration.

The successful deployment of DPPACs in these beam experiments, with stable operation and high detection efficiencies throughout the month-long campaign, represents an important advance and paves the way for future experiments at HIRFL-RIBLL1 and HIAF-HIRIBL.

V. SUMMARY AND PROSPECT

We have developed position-sensitive double parallel-plate avalanche counters (DPPACs) to measure trajectories, positions and incident angles of radioactive ion beams in nuclear physics experiments. The detectors were successfully deployed in a month-long experimental campaign at RIBLL1 using ^{10}Be and ^{10,11,16}C secondary beams, with two DPPACs placed upstream of the target for precise incident beam tracking. The results show excellent track reconstruction for target nuclei, and more importantly, long-term stable operation with >90% and close to 100% efficiencies for the respective DPPACs, confirming their high reliability for RI beam experiments. Future plans include larger DPPACs for secondary beam tracking at HIAF focal planes [10] and further optimization for heavier ions.

VI. ACKNOWLEDGMENTS

The authors thank the HIRFL staff for providing stable beams, and the HIRFL-RIBLL1 staff for technical support during the experiment with radioactive ion beams. The experiment was carried out as part of the campaign experiments of the LENG (Low temperature target system for Exotic Nuclei reactions with Gas) collaboration.

[1] Y. Yano, Nuclear Instruments and Methods in Physics Research Section B: Beam Interactions with Materials and Atoms **261**, 1009 (2007), the Application of Accelerators in Research and Industry.
[2] P. Spiller and G. Franchetti, Nuclear Instruments and Methods in Physics Research Section A: Accelerators, Spectrometers, Detectors and Associated Equipment **561**, 305 (2006), proceedings of the Workshop on High Intensity Beam Dynamics.
[3] J. Wei, H. Ao, S. Beher, *et al.*, International Journal of Modern Physics E **28**, 1930003 (2019).
[4] Z. Y. Sun, W. L. Zhan, Z. Y. Guo, *et al.*, Chin. Phys. Lett. **15**, 790 (1998).
[5] Z. Y. Sun, W. L. Zhan, Z. Y. Guo, *et al.*, Nucl. Instrum. Methods Phys. Res. Sect. A **503**, 496 (2003).
[6] J. W. Xia, W. L. Zhan, B. W. Wei, *et al.*, Nucl Instrum Meth A **488**, 11 (2002).
[7] B. H. Sun, J. W. Zhao, X. H. Zhang, *et al.*, Sci Bull **63**, 78 (2018).
[8] L. Sheng, X. Zhang, J. Zhang, *et al.*, Nuclear Instruments and Methods in Physics Research Section B: Beam Interactions with Materials and Atoms **469**, 1 (2020).
[9] L. Sheng, X. Zhang, H. Ren, *et al.*, Nuclear Instruments and Methods in Physics Research Section B: Beam Interactions with Materials and Atoms **547**, 165214 (2024).
[10] X. Zhou and J. Yang, AAPPS Bulletin **32**, 1 (2022).
[11] C. J. Horowitz, A. Arcones, B. Côté, *et al.*, Journal of Physics G: Nuclear and Particle Physics **46**, 083001 (2019).
[12] F. Nunes, G. Potel Aguilar, T. Poxon-Pearson, *et al.*, Annual Review of Nuclear and Particle Science **70**, 147 (2020).
[13] I. Tanihata, H. Hamagaki, O. Hashimoto, *et al.*, Physical Review Letters **55**, 2676 (1985).
[14] I. Tanihata, H. Savajols, and R. Kanungo, Prog. Part. Nucl. Phys. **68**, 215 (2013).
[15] T. Nakamura, H. Sakurai, and H. Watanabe, Progress in Particle and Nuclear Physics **97**, 53 (2017).
[16] D. T. Tran, H. J. Ong, G. Hagen, *et al.*, Nature Communications **9** (2018), 10.1038/s41467-018-04024-y.
[17] Y. Ye, X. Yang, H. Sakurai, *et al.*, Nature Review Physics **7**, 21 (2025).
[18] T. Kobayashi, F. Bieser, T. Symons, and D. Greiner, Nucl. Instrum. Meth. A **254**, 281 (1987).
[19] H. Miya, S. Ota, T. Fujii, *et al.*, Nucl. Instrum. Meth. B **317**, 701 (2013).
[20] Y. Z. Sun, Z. Y. Sun, S. T. Wang, *et al.*, Nuclear Instruments and Methods in Physics Research Section A: Accelerators, Spectrometers, Detectors and Associated Equipment **894**, 72 (2018).
[21] J. Cub, C. Gund, D. Pansegrau, *et al.*, Nuclear Instruments and Methods in Physics Research Section A: Accelerators,

Spectrometers, Detectors and Associated Equipment **453**, 522 (2000).
[22] H. Kumagai, A. Ozawa, N. Fukuda, *et al.*, Nuclear Instruments and Methods in Physics Research Section A: Accelerators, Spectrometers, Detectors and Associated Equipment **470**, 562 (2001).
[23] H. Kumagai, T. Ohnishi, N. Fukuda, *et al.*, Nuclear Instruments and Methods in Physics Research Section B: Beam Interactions with Materials and Atoms **317**, 717 (2013), xVIth International Conference on ElectroMagnetic Isotope Separators and Techniques Related to their Applications, December 2–7, 2012 at Matsue, Japan.
[24] C. Akers, K. B. Lee, Y. J. Kim, *et al.*, Journal of the Korean Physical Society **70**, 682 (2017).
[25] S. D. Carlo and M. Cortesi, Physical Review Accelerators and Beams **27**, 044801 (2024).
[26] V. Hlinka, M. Ivanov, R. Janik, *et al.*, Nuclear Instruments and Methods in Physics Research Section A: Accelerators, Spectrometers, Detectors and Associated Equipment **419**, 503 (1998).
[27] R. Janik, A. Prochazka, B. Sitar, *et al.*, Nuclear Instruments and Methods in Physics Research Section A: Accelerators, Spectrometers, Detectors and Associated Equipment **640**, 54 (2011).
[28] F. Garcia, T. Grahn, J. Hoffmann, *et al.*, Nuclear Instruments and Methods in Physics Research Section A: Accelerators, Spectrometers, Detectors and Associated Equipment **884**, 18 (2018).
[29] M. Luoma, F. García, J. Äystö, *et al.*, Nuclear Instruments and Methods in Physics Research Section A: Accelerators, Spectrometers, Detectors and Associated Equipment **1052**, 168262 (2023).
[30] H. Sann, H. Damjantschitsch, D. Hebbard, *et al.*, Nuclear Instruments and Methods in Physics Research Section A: Accelerators, Spectrometers, Detectors and Associated Equipment **124**, 509 (1975).
[31] J. Lai, L. Afanasieva, J. Blackmon, *et al.*, Nuclear Instruments and Methods in Physics Research Section A: Accelerators, Spectrometers, Detectors and Associated Equipment **890**, 119 (2018).
[32] A. Damyanova and A. Bravar, Nuclear Instruments and Methods in Physics Research Section A: Accelerators, Spectrometers, Detectors and Associated Equipment **845**, 475 (2017).
[33] M. Czogalik, C. Nociforo, M. Alfonsi, *et al.*, Journal of Instrumentation **19**, C06008 (2024).
[34] A. I. Stefanescu, V. Panin, L. Trache, *et al.*, **58**, 223 (2022).
[35] J. Christiansen, Z. Angew. Phys. **4**, 326 (1952).
[36] W. Seidel, H. Ortlepp, F. Stary, and H. Sodan, Nuclear Instruments and Methods in Physics Research Section A: Accelerators, Spectrometers, Detectors and Associated Equipment **273**, 536 (1988).
[37] Y. J. Zhou, P. Ma, J. S. Wang, *et al.*, Nuclear Physics Review **34**, 768 (2017).
[38] X. L. Wei, F. H. Guan, H. R. Yang, *et al.*, Nuclear Engineering and Technology **52**, 575 (2020).
[39] Y. J. Wang, F. H. Guan, Q. H. Wu, *et al.*, Physics Letters B **825**, 136856 (2022).
[40] X.-Y. Diao, F.-H. Guan, Y.-J. Wang, *et al.*, Nuclear Science and Techniques **33**, 40 (2022).
[41] Y. H. Qin, Q. L. Niu, D. Guo, *et al.*, Physics Letters B **850**, 138514 (2024).
[42] Z. H. Yang, Y. L. Ye, Z. H. Li, *et al.*, Physical Review Letters **112**, 162501 (2014).
[43] G.-L. Zhang, Y.-J. Yao, G.-X. Zhang, *et al.*, Nuclear Science and Techniques **28**, 104 (2017).
[44] Y. Liu, Y. L. Ye, J. L. Lou, *et al.*, Physical Review Letters **124**, 192501 (2020).
[45] Y. Jiang, J. L. Lou, Y. L. Ye, *et al.*, Physical Review C **101**, 024601 (2020).
[46] J. B. Ma, S. Terashima, H. J. Ong, *et al.*, Chinese Physics C **49**, 084001 (2025).
[47] K. Wei, *Study on the BEC-like State in* ^{14}C, Doctoral thesis, Peking University.
[48] Z. J. Li, X. L. Wei, Y. S. Yang, *et al.*, Journal of Instrumentation **19**, P02005 (2024).
[49] M. Zixu, Z. Weidong, L. Bingfeng, *et al.*, Nuclear Physics Review **42**, 482 (2025).
[50] XIA LLC, Pixie-16 user manual (issue 3.06) (2019).
[51] K.-J. Zhou, Z.-H. Yang, H.-J. Ong, *et al.*, submitted to Nuclear Science and Techniques.
[52] Z. Du, Z. Yang, H. Ge, *et al.*, submitted to Journal of Instrumentation.